

THE OUTSKIRTS OF DARK MATTER HALOS: DETAILED THEORETICAL PREDICTIONS

JUAN E. BETANCORT-RIJO¹, MIGUEL A. SANCHEZ-CONDE², FRANCISCO PRADA² AND SANTIAGO G. PATIRI¹

¹Instituto de Astrofísica de Canarias, Vía Láctea s/n, La Laguna, Tenerife, E38200, Spain and

²Instituto de Astrofísica de Andalucía (CSIC), E18008, Granada, Spain

draft ApJ, 29/09/05

ABSTRACT

In the present work we describe the formalism necessary to derive the properties of dark matter halos beyond two virial radius using the spherical collapse model (without shell crossing), and provide the framework for the theoretical prediction presented in Prada et al. (2005). We show in detail how to obtain within this model the probability distribution for the spherically-averaged enclosed density at any radii $P(\bar{\rho}; r)$. Using this probability distribution, we compute the most probable and mean density profiles, which turns out to differ considerably from each other. We also show how to obtain the typical profile, as well as the probability distribution and mean profile for the spherically averaged radial velocity. Two probability distributions are obtained: a first one is derived using a simple assumption, that is, if Q is the virial radius in Lagrangian coordinates, then the enclosed linear contrast $\bar{\rho}(q; Q)$ must satisfy the condition that $\bar{\rho}(q = Q) = \bar{\rho}_{vir}$; where $\bar{\rho}_{vir}$ is the linear density contrast within the virial radius R_{vir} at the moment of virialization. Then we introduce an additional constraint to obtain a more accurate $P(\bar{\rho}; r)$ which reproduces to a higher degree of precision the distribution of the spherically averaged enclosed density found in the simulations. This new constraint is $\bar{\rho}(q; Q) < \bar{\rho}_{vir}$ for $q > Q$, which means that there are no radii larger than R_{vir} where the density contrast is larger than that used to define the virial radius. Finally, we compare in detail our theoretical predictions for the probability distributions with the results found in the simulations.

Subject headings: cosmology:theory — dark matter — large-scale structure of universe — methods:analytical

1. INTRODUCTION

The study of the density profile of cold dark matter halos beyond the virial radius is a subject of considerable relevance. From an observational point of view, knowledge of the shape of the density profile far beyond the virial radius is essential for an appropriate interpretation of gravitational lensing phenomena (e.g. Smith et al. 2001; Guzik & Seljak 2002; Hoekstra et al. 2004; Sheldon et al. 2004), the pattern of Lyman alpha absorption around virialized systems (e.g. Barkana 2004; Bajtlik, Duncan & Ostriker 1988) as well as the motion of satellite galaxies as a test for dark matter distribution at large radii (Zaritsky & White 1994, Zaritsky et al. 1997; Prada et al. 2003, Brainerd 2004; Conroy et al. 2004). From the theoretical point of view, the study of the properties of dark matter halos at several virial radius in cosmological simulations provide an excellent benchmark for developing and testing the basic theoretical framework which will be decisive for a full understanding of the physical origin and formation of the Λ CDM halos.

Understanding halo properties involves a set of theoretical considerations. First, we have the issue of choosing the correct initial density profile. Furthermore, it is the question of which processes are relevant to the gravitational evolution of the initial profile: is only the spherical collapse what matters or is triaxiality important? up to which radius can we use the standard spherical collapse model without shell crossing? are highly asymmetrical processes, like merging, relevant? In order to answer these questions it is very convenient to focus first on those properties of the halos which involve the fewest theoretical uncertainties.

The dark matter density profiles at several virial radius are particularly suitable to check whether the spherical collapse model can provide accurate predictions (see Prada

et al. 2005). In fact, it has been shown that the spherical collapse model reproduces very well the relationship between the small values of the spherically-averaged enclosed density at those large distances and the radial velocity (Lilje et al. 1986).

We define the spherically-averaged enclosed density as:

$$\frac{\langle \bar{\rho} \rangle}{\bar{\rho}_m} = 1 +$$

where $\bar{\rho}$ is the enclosed density contrast and $\bar{\rho}_m$ the average matter density in the Universe. We can also define the spherically-averaged local density as:

$$\frac{\rho(r)}{\bar{\rho}_m} = 1 + \delta$$

where δ is the density contrast in a narrow shell of radius r . We can then obtain the density contrast δ from the enclosed density contrast using the relation:

$$\delta(r) = \frac{3}{r^2} \frac{d}{dr}(r^3 \bar{\rho}(r)):$$

Despite to all the effort done to understand the central dense regions of the dark matter halos in cosmological simulations, very little attention has been devoted to the study of the regions beyond the formal virial radius, i.e. the radius within which the spherically-averaged enclosed density is equal to some specific value. The main goal of the work presented in this paper is focused on the outskirts of the dark matter halos, where the correct evolution of the spherically-averaged enclosed density profiles can be obtained using the standard (without shell crossing) spherical collapse model. This model, first developed by Gunn & Gott (1972) and Gunn (1977), describes the collision-less collapse of a spherical perturbation in an expanding background. They introduced for the first time the cosmological expansion and the role of adiabatic invariance in the formation of individual objects. Later,

Fillmore & Goldreich (1984) found analytical predictions for the density of collapsed objects seeded by scale-free primordial perturbations in a flat universe. Hoffman & Shaham (1985) generalized these solutions to realistic initial conditions in flat and open Friedmann models. Some studies have been done to include more realistic dynamics of the growth process (e.g. Padmanabhan 1996; Avila-Reese, Firmani & Hernández 1998; Lokas 2000; Subramanian, Cen & Ostriker 2000).

There are plenty of works in the literature using the spherical collapse model to predict the density profiles of dark matter halos mainly focus to explain their central regions. For example Bertschinger (1985) used the spherical collapse with shell crossing to obtain the density profiles resulting from initial power law density profiles. Lokas & Hoffman (2000) considered more general initial profiles. The effect of non-radial motions has also been widely treated (see Ryden & Gunn 1987; Gurevich & Zybin 1988; Avila-Reese et al. 1998; White & Zaritsky 1992; Sikivie et al. 1997; Nusser 2001; Hiodelis 2001). Some of these authors have used arbitrary initial profiles, while others have assumed the mean initial profile around density maxima (Bardeen et al. 1986, BBKS). In all these works the angular momentum is introduced ad hoc, although more recently it has been done in a more natural way (Nusser 2001; Ascasibar et al. 2004). Concerning to the outer parts of the dark matter halos, only Barkana (2004) has adopted an appropriate initial profile, but only for a restricted type of density profile. The more recent work by Prada et al. (2005) have obtained a detailed prediction for the mean and most probable density profile and have provided a detailed comparison with cosmological simulations.

A proper understanding of the physics of dark matter halos involves to predict correctly not only the mean halo density profile for any given mass but also the whole probability distribution for the enclosed density contrast at any given radii, $P(\delta; r)$. A first attempt to determine it can be found in Prada et al. (2005), where it has been shown to be generally in good agreement with the cosmological simulations. Nevertheless, this probability distribution shows a long tail for large values of δ compared to that from simulations at any radius. In this paper we present a more accurate prediction for the probability distribution $P(\delta; r)$ that constitutes the main new result of this work. We also give in detail the theoretical background of the predictions presented in Prada et al. (2005). The agreement of our new predictions with the simulations is excellent even in the tail of the distribution. Furthermore, we also compute the radial velocity probability distribution and the mean radial velocity profile.

The work is organized as follows. In section 2 we present our theoretical framework and obtain the typical density profile of dark matter halos. In section 3 we show in detail how to obtain the probability distribution for the spherically-averaged enclosed density contrast at a given radii, $P(\delta; r)$, presented in Prada et al. (2005). The most probable and mean profiles are derived. In section 4, we compute the probability distribution and mean profile for the spherically averaged radial velocity. In section 5, we obtain a more accurate probability distribution than that used in the previous sections, and compare again with that found in the simulations. Final remarks are given in section 6.

2. THE TYPICAL DENSITY PROFILE OF DARK MATTER HALOS

The present spherically-averaged enclosed density profiles attains a density contrast value of δ_{vir} at certain radius, the so

called virial radius. At larger radii the density contrast must be, by definition, smaller than δ_{vir} , otherwise the virial radius would be larger than its nominal value.

We shall now make some comments on the values of δ_{vir} and r_{vir} the we use.

Although at several virial radius the spherically-averaged enclosed linear and actual densities are related by the spherical collapse model, the same does not apply within the virial radius. The spherically-averaged enclosed density contrast within one virial radius, δ_{vir} , and the corresponding enclosed linear density contrast, δ_{vir} , are not related as homologous quantities at larger radii, because at one virial radius shell crossing becomes important. Consequently, the value of δ_{vir} corresponding to $\delta_{vir}=340$ (the value we adopted to define the virial radius) is somewhat uncertain. As a result of work still in progress we will be able to provide the precise values for δ_{vir} and determine its possible small dependence on mass. Here we use for all masses $\delta_{vir}=1.9$, value that leads to very good results and that may be inferred from the fact that when $\delta_{vir}=180$, δ_{vir} is close to 1.68 for all cosmologies (Jenkins et al. 2001).

It must be noted that for all our predictions it is irrelevant whether the value of δ_{vir} that we use actually corresponds to the "virial" density contrast or not. For "virial" density contrast we mean the enclosed density contrast within the largest radii so that we have statistical equilibrium. The precise value of δ_{vir} is still problematic but, to our purposes, it can be chosen freely to define a conventional "virial radius". Since we have used numerical simulations with δ_{vir} equal to 340, we will take the same value by default in all the calculations.

Let $\delta_i(q; i)$ be a realization of the spherically-averaged initial enclosed density profile around a protohalo with a given present virial radius linearly extrapolated to the present, where q is the lagrangian distance from the center of the halo to the given point and i is an index running over realizations. Any realization of the initial profile may be transformed using the standard spherical collapse model (without shell-crossing). We can use the relationship found in the model between the linear value of the density contrast within a sphere, δ_l , and the actual density contrast within that sphere, δ (Sheth and Tormen (2002)):

$$\delta_l(\delta) = \frac{c}{1.68647} \delta^{1.68647} - \frac{1.35}{(1+\delta^2)^3} - \frac{1.12431}{(1+\delta)^2} + \frac{0.78785}{(1+\delta)^{5.8661}} \quad (1)$$

or, rather its inverse function $\delta(\delta_l)$ (Patiri et al.(2004) expression (4)):

$$\delta(\delta_l) = 0.993 \left[(1 - 0.607(\delta_l - 6.5 \cdot 10^{-3}(1 - \delta_l) + (\delta_l - 1.55))^2)^{-1.56} - 1 \right]$$

being δ the step function:

$$\delta(x) = \begin{cases} 1 & \text{if } x > 0 \\ 0 & \text{if } x = 0 \end{cases}$$

Transforming for every shell δ_l and q into δ and r (the Eulerian radius of the shell) we may obtain, in parametric form, the initial profile $\delta_l(q; i)$ spherically evolved, $\delta(r; i)$.

$$\delta(r; i) = \delta_l(q; i); \quad r = [1 + \delta_l(q; i)]^{1/3} q \quad (2)$$

This two equations gives $\delta(r; i)$ implicitly with q as parameter.

We must now eliminate all linear profiles leading to present profiles which attains a enclosed density contrast larger than (or equal to) $\bar{\rho}_{vir}$ at a radii larger than the nominal virial radius. The ensemble of remaining halos allow us to obtain the predictions of the standard spherical collapse model for any statistics. For example, we shall obtain the predictions for the mean profile:

$$\langle \rho(r) \rangle < \langle \rho(r;j) \rangle_j$$

That is, the average over all remaining halos (j runs over these halos). We shall also consider the most probable profile, $\rho_p(r)$, that is, the profile that associates with every value of r the value with the largest probability density.

The procedure described above to obtain the spherical model predictions (i.e. realizations evolved with expression (2)) serve mostly to the purpose of clarifying the meaning of those predictions and we only use it as a test to the analytical expressions. In practise, we shall use another procedure to obtain directly $\bar{\rho}(r)$, $\rho_p(r)$ and, in fact, the whole probability distribution for the value of ρ at a given value of r , $P(\rho; r)$.

Before dealing with the detailed predictions just mentioned we consider a simpler prediction which shall help clarifying the rest of the work, and which is related to previous approaches (Barkana 2004).

Consider the ensemble of all halos, $\langle \rho(r;j) \rangle_j$, attaining a value of $\bar{\rho}_{vir}$ at a virial radius and smaller values for larger radii. If we transform back these profile to their linear counterpart, we obtain the ensemble $\langle \rho(q;j) \rangle_j$. Let us now take the average over this ensemble (now for a fixed value of q):

$$\langle \rho(q) \rangle < \langle \rho(q;j) \rangle_j$$

Evolving this profile by means of the spherical collapse model we obtain a profile which we call typical profile and represent by $\rho_t(r)$, that is, this profile is simply the mean profile in the initial conditions spherically evolved.

Note that the typical density profile is defined because of its simplicity and not because it constitutes a prediction for any specific statistics of the actual halos. Nevertheless, it should not be very different from the most probable profile. Later we will study how these two profiles differ each other. This profile definition is the same as that used by Barkana (2004), but we use a different approximation to derive it.

To obtain the mean linear density profile $\bar{\rho}_l(q)$ subject to the condition that in the present enclosed density profile the virialization density contrast, $\bar{\rho}_{vir}$, is not attained beyond the virial radius, Barkana used barrier penetration results. He obtained the probability distribution for $\rho_l(q)$ given the conditions:

$$\rho_l(Q) = \bar{\rho}_{vir}; \quad \rho_l(q) < \bar{\rho}_{vir} \quad 8q > Q$$

$$Q = R_{vir}(1 + \bar{\rho}_{vir})^{1/3}$$

where R_{vir} is the virial radius (Q the corresponding Lagrangian radius), and $\bar{\rho}_{vir}$ is the linear counterpart of $\bar{\rho}_{vir}$. Then, by averaging over all ρ_l values smaller than $\bar{\rho}_{vir}$, he obtained the mean linear profile, $\bar{\rho}_l(q)$, with those conditions. However, he had to make some simplifications, the most relevant one a sharp filter in k -space, rather than the top hat filter which is the natural one in this context.

In our approach we first obtain the probability for $\rho_l(q)$ only with the condition $\rho_l(Q) = \bar{\rho}_{vir}$:

$$P(\rho_l; q) = P(\rho_l(q) = \rho_l(Q) = \bar{\rho}_{vir}) = \frac{\exp\left[-\frac{1}{2} \frac{(\rho_l(q) - \bar{\rho}_{vir})^2}{g}\right]}{\sqrt{2\pi} g^{1/2}} \quad (3)$$

where

$$g(q) = \frac{2}{2} - \frac{2}{1} \frac{12(q)}{12(Q)}$$

$$\langle \rho_l(x) \rangle^2 = \frac{1}{2} \int_0^{\infty} \langle \rho_l(k) \rangle^2 WT^2(xk) k^2 dk$$

$$12 = 12(q) = \frac{1}{2} \int_0^{\infty} \langle \rho_l(k) \rangle^2 WT(qk) WT(Qk) k^2 dk$$

$$WT(x) = \frac{3(\sin x - x \cos x)}{x^3}$$

where $\langle \rho_l(k) \rangle^2$ stands for the power spectra of the density fluctuations linearly extrapolated to the present.

It is convenient to use a simple and accurate approximation for $12(q)$:

$$\frac{12(q)}{12(Q)} = e^{-b(Q) \left(\frac{q}{Q}\right)^2 - 1} \quad (4)$$

where $b(Q)$ is a coefficient depending on the the size of the halo, Q :

$$b(Q) = -\frac{1}{2} \frac{d \ln \langle \rho_l(x) \rangle}{d \ln x} \Big|_{x=Q}$$

If no restriction other than $\rho_l(Q) = \bar{\rho}_{vir}$ were imposed on $\rho_l(q)$ the mean linear profile would be:

$$\bar{\rho}_l(q) = \int_{-1}^{\infty} P(\rho_l(q) = \rho_l(Q) = \bar{\rho}_{vir}) \rho_l(q) d(\rho_l(q)) = \bar{\rho}_{vir} \frac{12(q)}{12(Q)} \quad (5)$$

However, we are interested on the mean profiles satisfying also $\rho_l(q) < \bar{\rho}_{vir}$ for $q > Q$. So, we must use as mean profile:

$$\bar{\rho}_l(q) = \frac{\int_{-1}^{\bar{\rho}_{vir}} P(\rho_l(q) = \rho_l(Q) = \bar{\rho}_{vir}) \rho_l(q) d(\rho_l(q))}{\int_{-1}^{\bar{\rho}_{vir}} P(\rho_l(q) = \rho_l(Q) = \bar{\rho}_{vir}) d(\rho_l(q))}$$

$$= \bar{\rho}_l(q) - \frac{\bar{\rho}_{vir}^2 e^{-\frac{1}{2} \frac{(\bar{\rho}_{vir} - \bar{\rho}_{vir})^2}{g(q)}}}{1 - \frac{1}{2} \text{erfc} \left[\frac{\bar{\rho}_{vir} - \bar{\rho}_{vir}}{\sqrt{2} g(q)} \right]}$$

For arbitrarily massive halos $(Q) \ll 1$. So, since for the relevant q values ($q < Q$) $\bar{\rho}_l(q) < \bar{\rho}_{vir}$, $\rho_l(q)$ is simply given by $\bar{\rho}_l(q)$. However, for halos with $(Q) \gg 1$, $\rho_l(q)$ is substantially steeper than $\bar{\rho}_l(q)$, resulting in steeper present density profiles for smaller masses. This result has previously been advanced by Barkana (Barkana 2004) and have been confirmed by means for numerical simulations (Prada et al. 2005).

It must be noted that the profile given by expression (5) is not exactly the mean linear profile implicit in the definition of typical profile. Note that at each value of q , ρ_l is constrained to lay below $\bar{\rho}_{vir}$ but the probability distribution

where this constraint is imposed does not account for the fact that the profile lays below ρ_{vir} at any other value of q larger than Q . This is, however, a good approximation, because the most relevant part of the present density profile (to ≈ 10 virial radius) corresponds to a narrow region in Lagrangian coordinates ($\approx 1.5Q$). The value of ρ_l for q between Q and $1.5Q$ are strongly correlated. So, if we impose the condition $\rho_l < \rho_{vir}$ at, for example, $q = 1.25Q$, the probability that the same condition holds at any q is close to one.

Once we have $\rho_l(q)$ all we need to do is to evolve it with the spherical collapse model. Using equations (2) we may write (Patiri et al.(2004) expression (20)):

$$\rho(r) = \bar{\rho}_l(q); \quad q = r [1 + \rho(r)]^{\frac{1}{3}} \quad (6)$$

where the right hand side of this equation is simply the function defined in expression (2) evaluated at $\bar{\rho}_l(q)$ (given by expression (5)). For each value of r we must solve this equation for the variable $\rho(r)$. Applying the function defined in expression (1), which is the inverse of that defined in (2), to both sides of this equation we have:

$$\rho_l(\rho(r)) = \bar{\rho}_l(q); \quad q = r [1 + \rho(r)]^{\frac{1}{3}} \quad (7)$$

where the left hand side is expression (1) evaluated at $\rho(r)$. This equation is usually simpler to solve than Eq.(6) and is the one we used in Prada et al.(2005). The profile obtained in this way is the typical enclosed density contrast profile, $\rho_l(r)$. To obtain the typical density contrast profile, $\rho_l(r)$, we may use the relationship (13), given at the end of next section.

3. THE PROBABILITY DISTRIBUTION, $P(\rho; R)$, MOST PROBABLE AND MEAN PROFILES

At a given value of r the value of ρ takes different values, $(r; j)$, over the assemble of halos. The question now is which is the probability distribution of ρ over this ensemble, $P(\rho; r)$. As we saw in the previous section, this can be done, in principle, by making realizations of the initial profile, $\rho_l(q; i)$, and evolving them accordingly with equations (2). Let's assume, as a first approximation, that the realizations of the initial profile may be carried out by generating for each value of q a value of ρ_l accordingly with distribution (3). That is, we assume that the distribution of ρ_l is only conditioned by the fact that $\rho_l(Q) = \rho_{vir}$. We shall latter consider initial profiles with an additional constraint. With these realizations we can elaborate for each value of r a histogram for $P(\rho; r)$. There is, however, a direct analytical procedure to obtain $P(\rho; r)$ from the probability distribution for ρ_l (expression (3) in the present approximation).

ρ_l is a unique function of ρ (expression (2)). So, $P(\rho; r)$ could be obtained from (3) simply through the change of variable $\rho = \rho_l$. However, expressions (2) show that in transforming the initial profile not only is ρ_l transformed into ρ , but also q is transformed into r . Now, expression (3) gives the distribution of ρ_l at a fixed q value. But what we want to obtain is the distribution for ρ at a fixed r value. So, since the relationship between q and r depends on ρ (or ρ_l) itself, it is clear that the derivation of $P(\rho; r)$ from expression (3) (i.e. from $P(\rho_l; q)$) can not be as simple as described above.

Fortunately, there is a simple expression relating both probability distributions, which is valid as long as shell-crossing is not important:

$$P(\rho; r) = \frac{d}{d\rho_l} \int_{\rho_l(\rho)}^{\infty} P(\rho_l; q) d\rho_l \quad (8)$$

where $\rho_l(\rho)$ is given by expression (1) and $P(\rho_l; q)$ is the linear profile. Note that ρ enters not only on the integration limit but also in the integrand through q . The derivation of this relationship is given in Patiri et al.(2004) appendix B. In that work this relationship was derived in regard with void density profiles, so it had an slightly different form. However, the argument presented in that work leads directly to expression (8) if we change underdensity by overdensity and expansion by contraction. Using expression (3) for $P(\rho_l; q)$ we find:

Deriving it with respect to ρ and using the definition of the error complementary function:

$$P(\rho; r) = \frac{1}{\rho} e^{-F^2(\rho)} \frac{d}{d\rho} F(\rho) \quad (9)$$

$$F(\rho) = \frac{\rho_l(\rho) - \rho_0(q)}{\sqrt{2} g(q)}; \quad \rho_0(q) = \frac{12(q)}{2(Q)} \rho_{vir}$$

$$q = r [1 + \rho(r)]^{\frac{1}{3}}$$

We may obtain an analytical expression for $P(\rho; r)$ using approximation (4) for $\frac{12(q)}{2(Q)}$ and the following approximation for $g(q)$ (which enters $g(q)$):

$$g(q) \approx (1.65 \cdot 10^{-2} + 0.105(q h Mpc^{-1}))^{-\frac{1}{2}}$$

As mentioned before, expression (8) is valid as long as shell-crossing is not important. In Prada et al.(2005) we have found by mean of comparison with numerical simulations that, beyond three virial radius, the relevance of shell-crossing diminishes quickly. This relevance can be estimated a priori (i.e. without comparison with simulations) obtaining $P(\rho; r)$ directly through realizations of the initial profile accordingly with expression (3) and evolving them accordingly with equations (2). If shell-crossing were irrelevant, the $P(\rho; r)$ obtained in this way should be equal to that given by expression (9). The presence of certain amount of shell-crossing will cause the $P(\rho; r)$ obtained with realization to have a somewhat smaller maxima and a more extended tail than that given by (9). In this case none of the procedures gives the correct $P(\rho; r)$ because both assume that ρ is related to ρ_l by means of expression (1), which is inconsistent when shell-crossing is important. However, the difference between the results obtained with both procedures is of the same order of the difference between any of them and the profile obtained with a proper treatment of shell-crossing. Note that even this last $P(\rho; r)$ is not the real one, since, as we said before, we are generating the initial profile using only a two point distribution (expression (3)).

In figure 1 we compare the $P(\rho; r)$ obtained by the two procedures mentioned above for several values of r expressed in unit of the virial radius (that we denote by s). We also show the corresponding histogram obtained from the numerical simulations described in Prada et al.(2005). For $s = 2.5$, where there is massive shell-crossing, there is substantial difference between the results of both procedures. A considerable amount of probability is transferred from the most probable value to much larger values (≈ 100) causing the distribution obtained through the realizations to be bimodal. For

$s = 3.5$ there is still a small amount of shell-crossing causing the maxima obtained with both procedures to differ by roughly a 20%. For larger values of s this difference steadily diminishes.

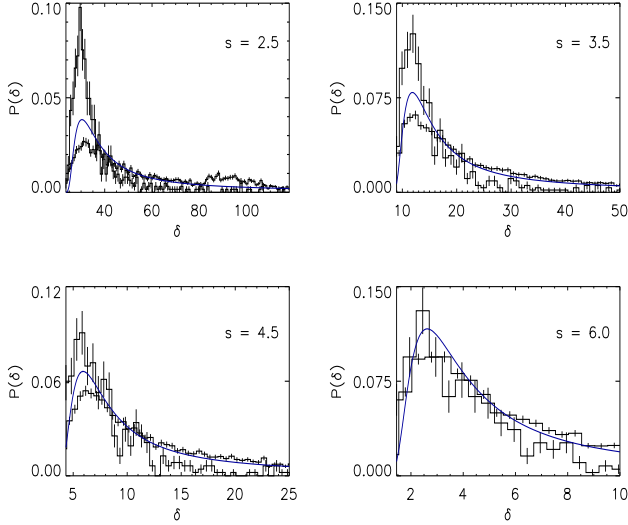


FIG. 1.— $P(\delta; r)$ as given by expression (9) compared with the corresponding histogram obtained through realizations (dark histogram) and that found in the simulations (light histogram) for four values of s ($r=R_{vir}$) and a mass of $3 \cdot 10^{12} h^{-1} M_{\odot}$ ($\sigma_{vir} = 340$ and $\sigma_{vir} = 1.9$).

Furthermore, as s increases the difference between the distribution given by expression (9) and the histogram obtained with the numerical simulations reduces. In fact, even for $s = 3.5$ the relative values of $P(\delta, r)$ at different values of δ to the left of the maxima are very well given by (9). The difference in the absolute values with respect to those in the histogram is due to the normalization. For δ values to the right of the maxima, expression (9) gives a considerably more extended tail than in the actual distribution. Therefore the normalization constant is larger in the latter case.

Note that, although the maxima of expression (9) and that of the histogram corresponding to the numerical simulations approach as s increases, due to the increasing irrelevance of the tail, this tail is still substantially more extended even for $s = 6$. Now, since the relevance of shell-crossing is small for s larger than 3, the most likely explanation for the excess in the tail given by expression (9) lays on the fact that we are using expression (3) for $P(\delta, r)$. In the last section we shall consider a better $P(\delta, r)$ and discuss the resulting improvement of the behaviour of its tail.

Using $P(\delta, r)$ (as given by (9)) we may immediately obtain the most probable and the mean profiles. For the first one we have:

$$P(\delta; r)_{max}; \quad \frac{d}{d\delta} P(\delta; r) = 0 \quad (10)$$

And for the mean profile, in principle:

$$\bar{\delta}(r) = \int_{-1}^{\infty} \delta P(\delta; r) d\delta \quad (11)$$

However, due to the fact that the mean is rather sensitive to the form of the tail, we must artificially cut off the tail. From

the simulations we know that the real tail practically ends at $\delta = \delta_0(r)$ with δ_0 given by:

$$P(\delta_0; r) = \frac{P(\delta_{max}; r)}{25}$$

So, instead of (11) we use (Prada et al.2005):

$$\bar{\delta}(r) = \frac{\int_{-1}^{\delta_0(r)} \delta P(\delta; r) d\delta}{\int_{-1}^{\delta_0(r)} P(\delta; r) d\delta} \quad (12)$$

In table 1 we give the values of δ_0 and δ_{max} for several values of s ($r=R_{vir}$). So far we have considered the probability distribution and profiles of the spherically-averaged enclosed density contrast, $\bar{\delta}$. We shall now consider the local density contrast δ' , that is the density contrast within a narrow shell of radius r . In this case we can not obtain $P(\delta', r)$ by mean of a simple relationship like expression (8). However, the mean δ' profile can be obtained from the mean $\bar{\delta}$ profile. To this end, note that for each actual density profile, that is, for each spherically evolved realization of the linear profile, $(r; j)$, the following relationship holds:

$$\delta'(r; j) = \frac{3}{r^2} \frac{d}{dr} (r^3 \delta(r; j)) \quad (13)$$

which follows immediately from the definitions of δ' and $\bar{\delta}$. The mean δ' profile does not correspond to any actual density profile. However, being the mean a linear operation, the same relationship holds for the mean profiles:

$$\begin{aligned} \bar{\delta}'(r) &= \langle \delta'(r; j) \rangle_j = \left\langle \frac{3}{r^2} \frac{d}{dr} (r^3 \delta(r; j)) \right\rangle_j \\ &= \frac{3}{r^2} \frac{d}{dr} (r^3 \langle \delta(r; j) \rangle_j) = \frac{3}{r^2} \frac{d}{dr} (r^3 \bar{\delta}(r)) \end{aligned} \quad (14)$$

TABLE 1
ARTIFICIAL CUT-OFF FOR $P(\delta; r)$

s	δ_{max}	δ_0
1.5	115.2	495.4
2.5	28.6	135.3
3.5	11.3	67.9
4.5	5.8	42.2
5.5	3.3	29.3
6.5	2.0	19.6
7.5	1.3	12.8
8.5	0.82	8.1

The most probable profile is constructed with the ensemble of profiles $(r; j)$ by means of a non-linear operation: that of choosing, for any value of r , the member of the ensemble with the largest probability density. So, relationship (13) is not valid between $\bar{\delta}'$ and $\bar{\delta}$, because the value of $\bar{\delta}$ at different values of r may correspond to different members of the ensemble. However, in Prada et al.(2005) we have used expression (13) to obtain $\bar{\delta}'(r)$ from $\bar{\delta}(r)$ and found results in good agreement with the simulations, but this is a posteriori agreement: unlike the prediction for $\bar{\delta}'(r)$, the value of $\bar{\delta}'(r)$ obtained using expression (13) is not a proper prediction.

4. RADIAL VELOCITY PROFILE OF DARK MATTER HALOS

In the spherical collapse model, the radial velocity at radii r with respect to the center of the spherical cloud is a unique

function of the spherically-averaged enclosed density contrast, $\bar{\rho}(r)$. An exact analytical expression may be given for this relationship using $\bar{\rho}(r)$ (expression (1)). Mass conservation within a shell with initial Lagrangian radius q , implies that, at any time, the following relationship must hold:

$$\frac{r(t)}{a(t)} = q(1 + \delta)^{\frac{1}{3}} \quad (15)$$

where $a(t)$ is the scale factor of the universe (normalized to 1 at present) so that the left hand side is the comoving radii of that shell at time t . Deriving this equation with respect to time we find:

$$\frac{\dot{r}(t)}{a(t)} - \frac{\dot{a}(t)}{a^2(t)} r(t) = \frac{\dot{r}(t) - H(t) r(t)}{a(t)} = -\frac{1}{3} q(1 + \delta)^{\frac{4}{3}} \quad (16)$$

where $H(t)$ is the Hubble constant. Using now (1) we may express δ in the form:

$$-\frac{d\delta}{d\ell} = \frac{D(t)}{D(t)} \delta; \quad \delta = \frac{D(t)}{D(a)} \ell = \frac{a}{D(a)} \frac{dD(a)}{da} H \ell \quad (17)$$

where $D(t)$ is the growing mode of linear density fluctuations. Now, since (1) is the inverse function of $\bar{\rho}(r)$ we have:

$$\frac{d\bar{\rho}(r)}{dr} = \frac{d\bar{\rho}(\ell)}{d\ell}^{-1}$$

Using this in (17), inserting (17) in (16) and using again (15) we find:

$$V_r = H(t) r - \frac{1}{3} \frac{aH}{D(a)} \frac{dD(a)}{da} \frac{r}{(1 + \delta)^{\frac{1}{3}}} \frac{\bar{\rho}(r)}{\frac{d\bar{\rho}(r)}{dr}} = r f(\bar{\rho}(r)) \quad (18)$$

For the concordant cosmology we have at present $H = 72 \text{ km/s/Mpc}$, $a = 1$, $\frac{dD(a)}{da} = D(a) = 0.51$. Writing (18) in the form $V_r = r f(\bar{\rho}(r))$ we may use expression (9) to obtain the probability distribution, $P(V_r; r)$, for V_r at radii r :

$$P(V_r; r) = P(\bar{\rho}(r)) = f^{-1} \left(\frac{V_r}{r}; r \right) \frac{df(\bar{\rho}(r))}{d\bar{\rho}(r)}^{-1} \quad (19)$$

where f^{-1} is the inverse function of f and where $P(\bar{\rho}(r))$ is given by expression (9).

This distribution should not be confused with the distribution of radial velocity of dark matter particles at a given value r . V_r is the mean radial velocity of all particles in a given narrow shell with radius r . So, for a given halo and a given value of r , V_r takes a unique value. Expression (19) gives the distribution of this value over the ensemble of halos.

The mean V_r profile is given by:

$$\bar{V}_r = \frac{\int_0^R P(\bar{\rho}(r)) r f(\bar{\rho}(r)) d\bar{\rho}(r)}{\int_0^R P(\bar{\rho}(r)) d\bar{\rho}(r)} \quad (20)$$

with $P(\bar{\rho}(r))$ given by (9), $\bar{\rho}(r)$ as defined in (7) and $f(\bar{\rho}(r))$ given by (18).

In figure 2 we show the predictions given by (20) for the mean radial velocity profile, and compare it with the profile:

$$V_r = r f(\bar{\rho}(r)) \quad (21)$$

That is, for each value of r , this expression gives V_r corresponding to the mean $\bar{\rho}$ at that r through Eq.(18). We find that Eq.(21) is a good approximation to Eq.(20).

Note that, although we have used the probability distribution given by Eq.(9), these expressions are valid for any $P(\bar{\rho}(r))$.

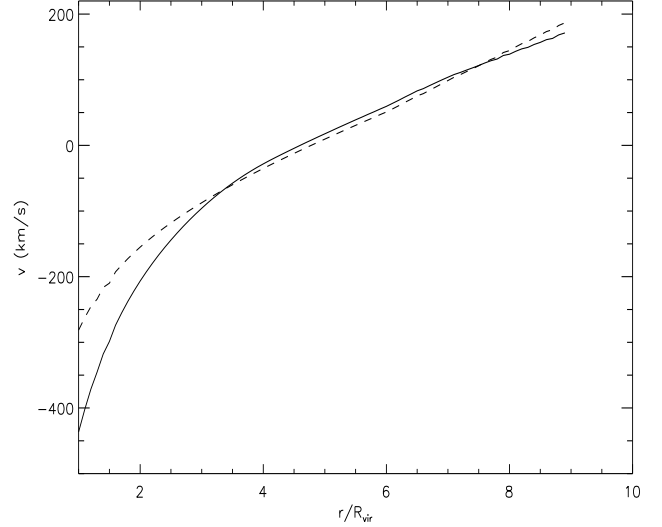


FIG. 2.— Radial velocity profile as given by expression (20) (filled line) and as given by expression (21) (dashed line). Both correspond to a mass of $3 \cdot 10^{12} h^{-1} M$

5. AN IMPROVED $P(\bar{\rho}(r); R)$

We have seen that for $s (= r/R_{vir})$ larger than 3 the mean difference between the actual value of $P(\bar{\rho}(r); r)$ (the histogram obtained from the simulations) and that given by expression (9) lays on the fact that we have used expression (3) for $P(\bar{\rho}(r); q)$. This distribution does not account for the fact that for all values of q larger than Q , $\bar{\rho}(r) < \bar{\rho}_{vir}$. Consequently, $P(\bar{\rho}(r); q)$ falls off with $\bar{\rho}(r)$ more slowly than it should and the same applies to $P(\bar{\rho}(r); r)$. We shall now consider a $P(\bar{\rho}(r); q)$ which takes into account this additional constraint.

We have already pointed out that the most relevant part of the present density profile (up to $s \approx 8$ virial radii) comes from a narrow band in Lagrangian coordinates (from Q to $s \approx 1.5Q$) so that the values of $\bar{\rho}(r)$ within this band are strongly correlated. This is the reason why using expression (3) for $P(\bar{\rho}(r); q)$ is a good approximation, because if $\bar{\rho}(r)$ at q lays below $\bar{\rho}_{vir}$ the same will probably be valid also at all q^0 larger than Q . We go now a step further and explicitly demand that $\bar{\rho}(r)$ lays below $\bar{\rho}_{vir}$ at all Lagrangian radii in between Q and q . Imposing the same condition at q^0 larger than q is unnecessary and will lead to a negligible change for $P(\bar{\rho}(r); q)$, because if $\bar{\rho}(r)$ lays below $\bar{\rho}_{vir}$ at q the same will occur at larger distances.

Given the strong correlation between the values $\bar{\rho}(r)$ in between Q and q (for the relevant q 's), the condition that for all values of q larger than Q , $\bar{\rho}(r) < \bar{\rho}_{vir}$, is almost equivalent to demanding that $\bar{\rho}(r)$ lays below $\bar{\rho}_{vir}$ at the middle point $q^0 = \frac{1}{2}(q + Q)$. We might have chosen any other point in the middle and searched for the point imposing the strongest constraint, since the real constraint must be stronger (i.e. the tail of the distribution falls off more steeply) than that imposed by the point leading to the strongest constraint. We have chosen the middle point because it seems a priori a good choice.

Here we discuss the main lines of the derivation and the result of $P(\bar{\rho}(r); q)$ within this new condition, which we represent by $P_1(\bar{\rho}(r); q)$. We give the details and the full descriptions of the expressions involved in appendix A.

To obtain $P_1(\bar{\rho}(r); q)$ we must first obtain the joint probability distribution for the value of $\bar{\rho}(r)$ at Q , the middle point, and at q .

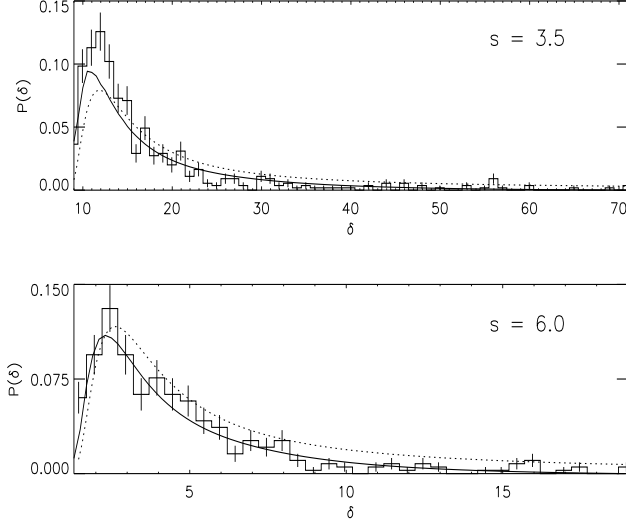


FIG. 3.— Probability distribution for δ at 3.5 and 6 virial radius for $3 \times 10^{12} h^{-1} M_{\odot}$. The filled curve corresponds to the approximation given by expression (23) and the dotted curve to that given by expression (9). The histogram corresponds to the same simulations as in fig.1.

We represent by x_1, x_2, x_3 respectively the value of δ at these three points.

The joint distribution for these three variables is a Gaussian trivariate distribution $P(x_1, x_2, x_3)$, which can be obtained for a given power spectra. With this distribution we may immediately obtain the distribution of x_3 conditioned to $x_1 = \delta_{vir}$, $x_2 < \delta_{vir}$, namely: $P_1(\delta; q)$. So, we have:

$$P_1(\delta; q) = \frac{\int_{-\delta_{vir}}^{\delta_{vir}} P(\delta_{vir}, x_2, x_3 = \delta) dx_2}{\int_{-\delta_{vir}}^{\delta_{vir}} P(\delta_{vir}, x_2) dx_2} \quad (22)$$

where $P(\delta_{vir}, x_2)$ is the joint probability distribution for x_1, x_2 with $x_1 = \delta_{vir}$ (see expression (3)).

The distribution for δ at fixed r within this formalism, which we represent by $P_1(\delta; r)$, may be obtained from $P_1(\delta; q)$ by means of expression (8), which is valid when shell-crossing is not important ($s \ll 3$):

$$P_1(\delta; r) = \frac{d}{dq} \int_{-\delta}^{\delta} P_1(\delta; q) d\delta \quad (23)$$

APPENDIX

DERIVATION OF $P_1(\delta; Q)$

The field of initial density fluctuations linearly extrapolated to the present $\delta(q)$ is a random Gaussian field. Any set of quantities obtained through a linear operation on a Gaussian field follows a Gaussian multivariate distribution. The quantities we are interested in are the average of the linear field within three concentric spheres centered at a randomly chosen point with Lagrangian coordinate q . The Lagrangian radius of these spheres are $Q, \frac{1}{2}(Q+q), q$ (note that q is not the norm of q) and we represent the average of the linear field within them by $x_1(q), x_2(q), x_3(q)$ respectively. These are three random Gaussian fields, but their values at a randomly chosen q we represent simply by x_1, x_2, x_3 . Their joint distribution is a Gaussian three-variate:

$$P(x_1, x_2, x_3) = \frac{e^{-\frac{1}{2} \mathbf{x}^T \mathbf{C}^{-1} \mathbf{x}}}{(2\pi)^{\frac{3}{2}} \det \mathbf{C}}$$

$$= \frac{1}{(2\pi)^{\frac{3}{2}} \det \mathbf{C}} \exp\left[-\frac{1}{2} \sum_{i,j=1}^3 C_{ij}^{-1} x_i x_j\right]; \quad (C)_{ij} = \langle \mathbf{x}_i \mathbf{x}_j \rangle$$

In figure 3 we show this probability distribution for a mass of $3 \times 10^{12} h^{-1} M_{\odot}$ at 3.5 and 6.0 virial radius. As expected, $P_1(\delta; r)$ falls off much faster than $P(\delta; r)$ being in excellent agreement with the simulations. Now it is not necessary to cut the tail of the distribution to obtain sensible results for the mean value of δ or higher order moments. $P_1(\delta; r)$ may be used in all expression in this work instead of $P(\delta; r)$ whenever high accuracy is needed.

6. FINAL REMARKS

The spherical collapse model describes very well the properties of dark matter halos beyond three virial radius. This could seem surprising given the fact that the density contours around halos may be considerably aspherical and the presence of tidal fields.

Nevertheless, the assumption that the spherically averaged density profiles at several virial radius evolves according with the spherical collapse model is not just a simplification introduced to make the problem tractable. The mean evolution is given by the spherical collapse model with some dispersion due to triaxiality. This has been shown by means of simulations (Lilje et al. 1986) and analytical works (Bernardeau 1994). At sufficiently large radii where δ is sufficiently small ($\delta \ll 10$) the dispersion becomes negligible. So studying the dark matter profile where the uncertainty of the evolution is small, we may check that the initial conditions we use are correct to a high degree of accuracy. With these conditions, as described by the most accurate probability distribution, $P_1(\delta; q)$, we should be able to obtain very accurate predictions for all possible definitions of density and velocity profile. That is, there is no room for remodeling; all properties must be explained with one and the same $P_1(\delta; q)$. Any residual discrepancy should be accounted for triaxiality, as we shall show in a future work. Going a step further, if we adequately take into account triaxiality and shell-crossing, the same initial conditions should explain the profile at radii. In this way, we could be able to explain the dark matter profiles at least down to a virial radii understanding the role played by the initial conditions and by the different processes relevant to the evolution.

ACKNOWLEDGMENTS

M.A. thanks support from PNAYA 2002-01241. We also thank support from the Spanish MEC under grant PNAYA 2005-07789.

where C^{-1} is the inverse matrix of C , whose diagonal elements are the variances of the x 's and the other elements are their correlations.

Using the definitions of the probability distribution for x_2 conditioned to a given value of x_1 , $P(x_2 | x_1)$, and of the distribution for x_3 conditioned to given values of x_1, x_2 , $P(x_3 | x_1, x_2)$, we may write:

$$P(x_1, x_2, x_3) = P(x_1) P(x_2 | x_1) P(x_3 | x_1, x_2) \quad (A1)$$

Now, by grouping terms in an appropriate manner we infer that:

$$P(x_1) = \frac{e^{-\frac{x_1^2}{2\sigma_1^2}}}{\sqrt{2\pi}\sigma_1}$$

$$P(x_2 | x_1) = \frac{e^{-\frac{(x_2 - Px_1)^2}{2g^2}}}{\sqrt{2\pi}g}$$

$$g = \frac{1}{2}(1 - \bar{c}_{12}^2); \quad P = \frac{\bar{c}_{12}}{1}$$

$$P(x_3 | x_1, x_2) = \frac{e^{-\frac{(x_3 - Ax_1 - Bx_2)^2}{2\varrho^2}}}{\sqrt{2\pi}\varrho} \quad (A2)$$

$$\varrho = \frac{1}{3} \frac{(1 + 2\bar{c}_{12}\bar{c}_{13}\bar{c}_{23} - (\bar{c}_{12}^2 + \bar{c}_{13}^2 + \bar{c}_{23}^2))}{(1 - \bar{c}_{12}^2)}$$

$$A = \frac{\bar{c}_{12}\bar{c}_{23} - \bar{c}_{13}}{1 - \bar{c}_{12}^2} \frac{3}{1}$$

$$B = \frac{\bar{c}_{12}\bar{c}_{13} - \bar{c}_{23}}{1 - \bar{c}_{12}^2} \frac{3}{2}$$

$$\bar{c}_{ij} = \frac{\langle x_i x_j \rangle}{\sigma_i \sigma_j}; \quad i, j \quad (q_i)$$

$$q_1 = Q; \quad q_2 = \frac{1}{2}(Q + q); \quad q_3 = q$$

(q) is the linear RMS density fluctuation as a function of Lagrangian radii (see expression (3)). $\langle x_i x_j \rangle$ is what we called ij in expression (3).

We may now obtain the distribution for x_3 conditioned to $x_1 = vir, x_2 < vir$:

$$P(x_3 | x_1 = vir, x_2 < vir) = \frac{\int_{-1}^R P(x_2 | x_1) P(x_3 | x_1, x_2) dx_2}{\int_{-1}^{vir} P(x_2 | x_1) dx_2} \quad (A3)$$

Note that $P(x_1)$ cancels.

Using (A2) and rearranging terms in the exponent we may write:

$$P(x_2 | x_1) P(x_3 | x_1, x_2) = \exp \left\{ -\frac{(x_3 - Ax_1)^2}{2\varrho^2} - \frac{P^2 x_1^2}{2g^2} + \frac{(\frac{Px_1}{2g} + \frac{Bx_3}{2\varrho} - \frac{ABx_1}{2\varrho})^2}{\frac{B^2}{2\varrho^2} + \frac{1}{2g}} \right\}$$

$$\exp \left\{ -\frac{B^2}{2\varrho^2} + \frac{1}{2g} \right\} \exp \left\{ -x_2^2 - \frac{(\frac{Px_1}{2g} + \frac{Bx_3}{2\varrho} - \frac{ABx_1}{2\varrho})^2}{\frac{B^2}{2\varrho^2} + \frac{1}{2g}} \right\}$$

x_2 appears only in the second factor and both integrals in (A3) can directly be expressed in terms of the error complementary function:

$$P(x_3 | x_1 = vir, x_2 < vir) = \frac{1}{\sqrt{2\pi}g^{\frac{1}{2}}L^{\frac{1}{2}}} \exp \left\{ -\frac{(x_3 - A vir)^2}{2\varrho^2} - \frac{P^2 vir^2}{2g^2} + \frac{U^2}{L} \right\}$$

$$1 - \frac{1}{2} \operatorname{erfc} \left(\frac{vir - U}{L} \right) L^{\frac{1}{2}} \quad 1 - \frac{1}{2} \operatorname{erfc} \left(\frac{vir(1-P)}{\sqrt{2}g^{\frac{1}{2}}} \right)^{-1}$$

$$U = \frac{vir P}{2g} + \frac{B x_3}{2 \varpi} - \frac{AB}{2} \frac{vir}{\varpi}$$

$$L = \frac{B^2}{2 \varpi} + \frac{1}{2g}$$

$P_1(r; q)$ is simply given by:

$$P_1(r; q) = P(x_3 = r \mid x_1 = vir, x_2 < vir)$$

Note that the left hand side depends on q through \bar{c}_{ij} . These quantities may be computed directly with arbitrary precision evaluating the integral entering their definition (expression (1)). However, to be able to obtain efficiently $P_1(r; q)$, we need accurate fits to these quantities as a function of q . It is very difficult, however, to obtain consistent approximation for these quantities: very small errors in \bar{c}_{ij} may lead to inconsistent result, for example, negative values for ϖ . So, it is more expedient to fit directly the quantities (A, B, P, ϖ) where the \bar{c}_{ij} enter. We find the following fits:

$$A = -e^{-1.386 b \left(\frac{q}{Q}\right)^2 - 1} \frac{3}{1}$$

$$B = 1 + e^{-1.504 b \left(\frac{q}{Q}\right)^2 - 1} \frac{3}{2}$$

$$P = e^{-0.475 b \left(\frac{q}{Q}\right)^2 - 1} \quad (A4)$$

$$\varpi = \frac{2}{3} \frac{6.63 \cdot 10^{-2} b^4 \left(\frac{q}{Q}\right)^2 - 1}{1 - \frac{1}{2} P}^4$$

where b is as defined in expression (3) ($b = 0.2544$ for $M = 3 \cdot 10^{12} h^{-1} M_\odot$).

REFERENCES

- Avila-Reese, V., Firmani, C. & Hernandez, X. 1998, *ApJ*, 505, 37
 Ascasibar, Y., Yepes, G., Gottloeber, S. & Mueller, V. 2004, *MNRAS*, 352, 1109
 Bajtlik S., Duncan R. C., Ostriker J. P., 1988, *ApJ*, 327, 570
 Bardeen, J. M., Bond, J. R., Kaiser, N. & Szalay, A. S. 1986, *ApJ*, 304, 15 (BBKS)
 Barkana R., 2004, *MNRAS*, 347, 59
 Bernardeau, F. 1994, *ApJ*, 427, 51
 Bertschinger, E. 1985, *ApJS*, 58, 39
 Brainerd, T.G., 2004, *astro-ph/0409381*
 Conroy, C., Newman, J. A., Davis, M., Coil, A. L., Yan, R., Cooper, M. C., Gerke, B. F., Faber, S. M., & Koo, D. C., 2004, *astro-ph/0409305*
 Fillmore, J. A. & Goldreich, P. 1984, *ApJ*, 281, 1
 Gunn, J. E. & Gott, J. R. 1972, *ApJ*, 176, 1
 Gunn J. E., 1977, *ApJ*, 218, 592
 Gurevich, A. V. & Zybin, K. P. 1988, *ZHETF*, 94, 3
 Guzik, J., & Seljak, U., 2002, *MNRAS*, 335, 311
 Hoekstra, H., Yee, H. K. C., Gladders, M. D., 2004, *ApJ*, 606, 67
 Hiotelis, N. 2002, *ã*, 382, 84
 Hoffman Y., Shaham J., 1985, *ApJ*, 297, 16
 Jenkins A., Frenk C. S., White S. D. M., Colberg J. M., Cole S., Evrard A. E., Couchman H. M. P., Yoshida N., 2001, *MNRAS*, 321, 372
 Lilje, P.B., Yahil, A. & Jones, B.J.T. 1986, *ApJ*, 307, L91
 Lokas E. L., 2000, *MNRAS*, 311, 423
 Lokas, E. L. & Hoffman, Y. 2000, *ApJ*, 542, L139
 Nusser, A. 2001, *MNRAS*, 325, 1397
 Padmanabhan T., 1996, *MNRAS*, 278, L29
 Patiri S., Betancort-Rijo J. E. & Prada F. 2004, *astro-ph/0407513*
 Prada, F., Vitvitska, M., Klypin, A., Holtzman, J. A., Schlegel, D. J., Grebel, E. K., Rix, H.-W., Brinkmann, J., McKay, T. A., & Csabai, I., 2003, *ApJ*, 598, 260
 Prada F., Klypin A. A., Simmoneau E., Betancort-Rijo J., Patiri S. G., Gottlöber S., Sanchez-Conde M. A., 2005 *astro-ph/0506432*
 Ryden, B. S. & Gunn, J. E. 1987, *ApJ*, 318, 15
 Sheldon, E. S., et al., 2004, *AJ*, 127, 2544
 Sheth, R. K. & Tormen, G. 2002, *MNRAS*, 329, 61
 Sikivie, P., Tkachev, I. I. & Wang Y. 1997, *Phys. Rev. D*, 56(4), 1863 .
 Smith, D. R., Bernstein, G. M., Fischer, P., & Jarvis, M., 2001, *ApJ*, 551, 643
 Subramanian K., Cen R., Ostriker J. P., 2000, *ApJ*, 538, 528
 White, S. D. M. & Zaritsky, D. 1992, *ApJ*, 394, 1
 Zaritsky, D. & White, S. D. M. 1994, *ApJ*, 435, 599
 Zaritsky, D., Smith, R., Frenk, C., & White, S. D. M. 1997, *ApJ*, 478, 39